Stanley, P., & Carver, J. P. (1977) *Proc. Natl. Acad. Sci. U.S.A. 74*, 5056–5059.
Staros, J. V., Bayley, H., Standring, D. N., & Knowles, J. R. (1978) *Biochem. Biophys. Res. Commun. 80*, 568–572.
Traut, R. R., Bollen, A., Sun, T., Hershey, J. W. B., Sunberg, J., & Pierce, L. R. (1973) *Biochemistry 12*, 3266–3273.
Wang, J. L., Cunningham, B. A., & Edelman, G. M. (1971) *Proc. Natl. Acad. Sci. U.S.A. 68*, 1130–1134.

Aggregation-Linked Kinetic Heterogeneity in Bovine Cardiac Myosin Subfragment 1†

Duane P. Flamig‡ and Michael A. Cusanovich*

ABSTRACT: Studies of the cardiac myosin subfragment 1 concentration dependence of the rate constants for adenosine 5′-triphosphate (ATP) binding and steady-state hydrolysis reveal that the observed rate constants are remarkably dependent on the protein concentration. The kinetics for ATP binding are biphasic, and both the fast- and slow-phase rate constants and the respective fractions of fast and slow material vary as a function of protein concentration. Two different types of kinetic experiments were conducted, one in which the ATP concentration was fixed but the subfragment 1 concentration was varied and another for which the ATP/subfragment 1 ratio was fixed but both concentrations were varied. The results of these two experiments on cardiac subfragment 1 are consistent with an ATP-dependent reversible aggregation. Light-scattering experiments confirm the presence of this aggregation and the ATP dependence. Similar studies on rabbit skeletal subfragment 1 give monophasic, protein-independent kinetics consistent with a monomeric species in solution. A simple monomer–dimer mechanism can account for the cardiac subfragment 1 kinetic results when changes in tryptophan fluorescence are used. However, the light-scattering results show that cardiac myosin subfragment 1 undergoes multiple reversible molecular weight changes in solution and may be tetrameric at high concentrations.

The binding of nucleotides to bovine cardiac myosin and subfragment 1 has previously been shown to be biphasic (Taylor & Weeds, 1976). Preliminary studies in our laboratory on cardiac S1[1] have confirmed the biphasic kinetics and indicated that relative amounts of the two kinetic species as well as the corresponding rate constants were dependent on the S1 concentration. According to the proposed three-step mechanism for the binding and rapid hydrolysis of ATP by myosin

$$M + ATP \overset{1}{\rightleftharpoons} MATP \overset{2}{\rightleftharpoons} M^{**}ADP{\cdot}P_i$$

the observed rate constants should be independent of the concentration of myosin under pseudo-first-order conditions for ATP with respect to myosin. The simplest explanation for the observed biphasic kinetics of bovine cardiac S1 is that two protein species are present with each binding ATP with a different rate constant. However, this model predicts that the fractions of fast and slow material should be constant for all nucleotide concentrations, which is contrary to what is observed with cardiac S1. The next simplest model is to assume that there is protein–protein interaction, the simplest type being reversible aggregation. The fact that cardiac myosin has complex kinetics has limited studies on this form of myosin. In an attempt to resolve this problem in order to make cardiac myosin more amenable to detailed study, we have investigated the kinetic and aggregation properties of cardiac S1.

Initially, a series of experiments were designed in which the ATP concentration was held constant, and the protein concentration was varied and the apparent rate constant for ATP binding was measured. If the interconversion of the two forms of the protein is slow compared to nucleotide binding, then the fractions of fast and slow material will yield the monomer–aggregate equilibrium constant directly as well as the binding rate constants for at least two forms of the protein. The ATP concentration was chosen at an intermediate value (60 μM) in order to maximize the effect of S1 concentration on the observed biphasic binding reaction. Since it was observed that the fraction of fast material increased with increasing ATP concentration at a fixed protein concentration, a second set of experiments was carried out in which the ATP/S1 ratio was held constant by simultaneously varying both reactant concentrations. This experiment was designed to further discriminate between protein concentration dependent aggregation and ATP-induced dissociation. The observed increase in the contribution of the fast species with increasing ATP concentration suggests that the interconversion of the two or more forms of S1 is competitive with nucleotide binding to the active site. When the ATP/S1 ratio is kept small but still almost pseudo first order, the nucleotide-induced interconversion can be minimized.

Taylor & Weeds (1976) have shown from steady-state phosphate release experiments as a function of ATP concentration that there are at least two forms of bovine cardiac

† From the Department of Biochemistry, University of Arizona, Tucson, Arizona 85721. *Received January 19, 1981; revised manuscript received June 10, 1981.* This work was supported by National Institutes of Health Grant HL-20984 and by a Muscular Dystrophy Postdoctoral Fellowship to D.P.F.
‡ Present address: Department of Chemistry, University of Oregon, Eugene, OR 97403.

[1] Abbreviations used: S1, subfragment 1; ATP, adenosine 5′-triphosphate; ATPase, adenosine-5′-triphosphatase; BTP, bis(Tris)propane, 1,3-bis[[tris(hydroxymethyl)methyl]amino]propane; DTT, dithiothreitol; Tris, tris(hydroxymethyl)aminomethane; EDTA, ethylenediaminetetraacetic acid; DEAE, diethylaminoethyl; $NaDodSO_4$, sodium dodecyl sulfate; LC, light chain; PM, photomultiplier.

0006-2960/81/0420-6760$01.25/0

myosin and that ion-exchange chromatography in the presence of pyrophosphate partially removes one of the species (or at least alters V_{max}). They have also observed the presence of aggregation in the ultracentrifuge. Thus, a third set of experiments was designed, involving the mixing of various concentrations of cardiac S1 with stoichiometric amounts of ATP, and the single turnover of ATP by tryptophan fluorescence changes was observed. These experiments allow the effect of aggregation on the rate-limiting step of the myosin ATPase mechanism to be established and related to effects on nucleotide binding. Finally, light-scattering experiments were conducted both in the absence and in the presence of ATP to measure the extent of nucleotide-linked reversible aggregation in bovine cardiac S1.

Materials and Methods

The following chemicals were from Sigma Chemical Co.: ATP, Sigma Grade (vanadium free); α-chymotrypsin, Type I-S; bis(Tris)propane [1,3-bis[[tris(hydroxymethyl)methyl]-amino]propane]; DTT. The $(NH_4)_2SO_4$ used was enzyme grade from Schwarz/Mann. All other chemicals were reagent grade.

The concentration of myosin was determined by using $A^{1\%}_{280}$ = 5.33 cm^{-1}, a light-scattering correction of 1.4 A_{320}, and a molecular weight of 468 000. The concentration of S1 was determined by using $A^{1\%}_{280}$ = 7.5 cm^{-1}, a light-scattering correction of 1.7 A_{320}, and a molecular weight of 115 000.

Preparation of Cardiac Myosin. The preparation of cardiac myosin that was used is a modification based on that of Taylor & Weeds (1976). All protein preparations and manipulations were performed at 4 °C. Well-trimmed left ventricles were minced in a meat grinder with $^1/_8$ in. holes. The mince was then homogenized and washed 3 times with 3 volumes of 50 mM KCl, 20 mM Tris/HCl, pH 7.5, 2 mM EDTA, and 1 mM DTT. The homogenized mince was then extracted for 1 h with stirring in 3 volumes of 0.3 M KCl, 0.15 M KH_2PO_4, 2 mM $Na_4P_2O_7$, 1 mM EDTA, 3 mM $MgCl_2$, and 2 mM ATP, pH 6.8. The extraction mixture was then centrifuged (5000*g*), and the supernatant was precipitated in 10–12 volumes of cold distilled H_2O. A second extraction was then done overnight with stirring in 0.3 M KCl and 0.1 M $Na_4P_2O_7$, pH 6.8, the extraction mixture was centrifuged, and the supernatant was precipitated in cold H_2O as for the first extraction. The pellets were then redissolved with an equal volume of 1.0 M KCl, 20 mM potassium phosphate, and 1 mM EDTA, pH 7.0, and centrifuged at 50000*g* for 1 h. The clear supernatant was then reprecipitated in 10–12 volumes of cold distilled H_2O. After an additional cycle of dissolution, high-speed centrifugation, and precipitation in cold H_2O, the pellets were dissolved in an equal volume of 1.0 M KCl, 20 mM phosphate, and 1 mM EDTA, pH 7.0, glycerine was added to 50% (v/v), and the mixture was stored at −20 °C.

The two extractions yielded myosins with identical Mg-ATPase activities. The yield of the second extraction was usually twice that of the first extraction, and S1 obtained from myosin from one or two extractions was kinetically identical. The total combined yield was generally 30–35 g of myosin/kg of mince. The double-extraction procedure gave yields of rabbit skeletal myosin also on the order of 35 g of myosin/kg of mince.

Preparation of Cardiac Myosin Subfragment 1. Attempts at preparation of cardiac S1 using chymotrypsin according to the procedure of Weeds & Taylor (1965) gave very low yields of S1. In addition, this procedure produced S1 with only a 16–17% maximum fluorescence enhancement upon ATP binding at pH 7.0 in 0.1 M KCl and 10 mM $MgCl_2$.

High yields of S1 could be obtained by digestion of myosin (10–20 mg/mL) in 0.5 M KCl, 10 mM potassium phosphate, and 0.5 mM EDTA, pH 7.0, with a 1:200 ratio (w/w) of chymotrypsin to myosin. The digestion was carried out for 16 h with stirring at 4 °C. Phenylmethanesulfonyl fluoride in ethanol was added to 5×10^{-4} to stop the digestion. The digest was successively precipitated at 35%, 45%, and 65% saturated ammonium sulfate by the addition of solid $(NH_4)_2SO_4$. The 35% precipitate contained a small amount of residual myosin and light meromyosin fragments, and the 45% precipitate contained heavy meromyosin plus fragments. The 65% precipitate which contained S1 plus fragments was dialyzed at 4 °C in 10 mM bis(Tris)propane–HCl and 0.1 mM DTT, pH 6.8 (at 23 °C), and applied to a DEAE-cellulose column equilibrated in the same buffer at 4 °C. The column was washed with several column volumes of loading buffer, and the S1 was then eluted with a 0–0.1 M KCl gradient in the same buffer. The peak tubes were eluted at 0.05 M KCl. A simpler procedure was to use a step jump to 0.05 M KCl after the wash. The fractions from the single peak containing S1 were pooled, and the S1 was precipitated by the addition of solid $(NH_4)_2SO_4$ to 65% saturation. The pellets were dissolved in a minimum volume of 1.0 M KCl, 20 mM potassium phosphate, and 1 mM EDTA, pH 7.0, glycerine was added to 50% (v/v), and the mixture was stored at −20 °C.

The effect of glycerine storage on the biphasic kinetics during the course of this study was shown to be negligible. Control experiments were done by following the kinetics of 4 μM cardiac S1 reacting with 25 and 200 μM ATP after mixing for each batch brought out of storage. The kinetic traces could be overlayed for both the 25 and 200 μM ATP experiments for cardiac S1 that had been stored for 2, 6, 8, 16, 26, and 60 weeks in 50% glycerine, 0.25 M KCl, 5 mM phosphate, and 0.25 mM EDTA, pH 7.0, at −20 °C. From these control experiments it is seen that the aggregation phenomena are not due to aging in the glycerine storage as identical kinetics were observed for up to 60 weeks of storage.

$NaDodSO_4$–polyacrylamide gels (10%) run according to Weeds & Taylor (1975) and Weeds et al. (1975) in a thin slab apparatus showed the presence of only one light chain, LC_1 (Weeds & Pope, 1977). The other light chain, LC_2, is completely removed with chymotrypsin treatment. LC_1 from S1 ran parallel to the same light chain from undigested myosin. The yield of S1 from 10 g of myosin was typically 2–3 g, and the remainder of active sites was in the form of heavy meromyosin. The production of S1 by this low-temperature, high-salt chymotrypsin digestion proceeds through the heavy meromyosin intermediate as suggested by Weeds & Pope (1977). Subfragment 1 produced by this method reproducibly gave 34–36% fluorescence enhancement upon ATP binding in 0.1 M KCl at pH 7.0. Rabbit skeletal chymotryptic S1 (A1) was prepared according to the method of Weeds & Taylor (1975).

Transient Kinetic Apparatus and Data Collection. A Durrum Model D-110 stopped-flow apparatus was modified by the addition of a xenon lamp housing with a Wotan XBO-150-W xenon lamp and a regulated dc high-voltage power supply and starter Model XL150 from OLIS (On-Line Instruments System, Jefferson, GA). Excitation was at 295 nm (6-nm bandwidth) from the Durrum prism monochromator. Fluorescence emission was detected at 90° with an EMI 9524S (EMI Gencom Inc.) photomultiplier (Kepco, Inc., dc regulated voltage supply for PM dynode). The emitted light was prefiltered with a Corning CS 7-51 colored glass filter (Corning Glass Works) to remove excitation light and isolate

the tryptophan emission band.

The photomultiplier current was converted to voltage and RC filtered with the Durrum Model D-131 amplifier. The resulting voltage was digitized in a Model 3600 OLIS interface coupled with a Data General Corp. NOVA 2 minicomputer. The resulting digitized waveform was then stored on a floppy disc (Xebec Model XFD-100) for further analysis. For each nucleotide concentration, 8–10 replications of 200 data points were averaged on line, and the resulting 200-point curve was stored for further analysis. The photomultiplier dynode voltage was typically 320 V which gave an amplifier output of 6 V for a 4 μM S1 concentration and a 0.12 V buffer background which was routinely subtracted for each experiment.

The temperature was regulated at 20 ± 0.1 °C for all kinetic experiments. The protein was kept on ice for the duration of the experiments. The drive syringes were filled and allowed to equilibrate to 20 °C in the stopped-flow apparatus which took about 10 min in our apparatus. The protein showed a remarkable time-dependent decrease in fluorescence enhancement upon nucleotide binding when incubated at 20 °C. The rate constants, however, were not effected. The above procedure minimized this effect so that all kinetic results are given at 10-min incubation time from 4 to 20 °C.

Transient Kinetic Data Reduction. The digitized voltages from the photomultiplier tube were converted to Δ voltages: $\Delta V_t = v_t - v_\infty - v_b$, where v_t is the voltage at any time t after mixing, v_∞ is the voltage at the end of the reaction and was collected after 10 s to be sure that the base line was stable and that the reaction was over, and v_b is the voltage of the buffer plus ATP background fluorescence. The Δ voltages, ΔV_t, were then fit to a sum of two exponentials, $\Delta V_t = a_1 \exp(-k_1 t) + a_2 \exp(-k_2 t)$. The method of Foss (1970) was used to provide initial guesses for a_1, k_1, a_2, and k_2, which were refined in a nonlinear least-squares routine employing unitary transformations and scaling to solve the Gaussian matrix equations (Greenstadt, 1967).

Since the myosin–ATP complex is more fluorescent than myosin and there is no detectable lag phase, both a_1 and a_2 are negative. The extrapolated fractional total amplitudes were then calculated by $\Delta Fl = [a_1 \exp(+k_1 t_d) + a_2 \exp(+k_2 t_d)]/\Delta V_0$, where t_d is the stopped-flow mixing dead time and is 3.5 ms for the instrument used, and $\Delta V_0 = v_\infty - v_b + a_1 \exp(+k_1 t_d) + a_2 \exp(+k_2 t_d)$, which represents the fluorescence of myosin in the absence of nucleotide. The extrapolated fractional fast- and slow-phase amplitudes were calculated by fraction fast $= a_1 \exp(+k_1 t_d)/[a_1 \exp(+k_1 t_d) + a_2 \exp(+k_2 t_d)]$ and fraction slow $= a_2 \exp(+k_2 t_d)/[a_1 \exp(+k_1 t_d) + a_2 \exp(+k_2 t_d)]$.

A two-exponential nonlinear least-squares fit was superior to a single-exponential fit for all of the ATP binding data to cardiac S1 with respect to the sum of squared residuals, run of residuals, and estimated parameter errors from the covariance matrix. In the case of rabbit skeletal S1 (A1), two exponentials could not be found so the data were fit with the single-exponential method of Foss (1970). Single-turnover experiments were conducted by flowing a nearly stoichiometric amount of ATP against various concentrations of S1. The entire fluorescence signal including the initial ATP binding was collected, and only the decay following the plateau phase was fit to exponentials. The single-turnover data could not be fit to two exponentials, so a single-exponential fit (with only three runs of residuals) was used for further analysis.

For determination of the effect of not having strict pseudo-first-order behavior of ATP with respect to S1, the following simple mechanism was used to generate curves which were then fit to single and double exponentials: $M + ATP \xrightarrow{k} M^*ATP$. The simulated normalized fluorescence change is given by $\Delta Fl = 1 - X_t/M_0$, where $X_t = M_0 ATP_0[\exp[(M_0 - ATP_0)kt] - 1]/[M_0 \exp[(M_0 - ATP_0)kt] - ATP_0]$, and M_0 and ATP_0 are the initial concentrations of S1 and ATP, respectively, with $ATP_0 > M_0$. Two-hundred evenly spaced times were used, and the total time was such that ΔFl was 95% complete. In the case where ATP/S1 = 3.6, the simulated curves slow down with time and hence will appear biphasic. However, meaningful double-exponential fits which describe the observed decrease in rate constants with increasing S1 concentrations for cardiac S1 could not be obtained. Since the simulated data could not successfully be fit by two exponentials for all variations of S1 and ATP concentrations used experimentally, the second-order rate constant, k, was varied until a single exponential, k_{obsd}, was obtained which fit the fast-phase rate constant at the largest ATP/S1 ratio for either cardiac or rabbit S1. The single-exponential fits to the simulated data are shown in Figures 1, 2, and 4 under Results.

Static Light Scattering. The apparent weight-average molecular weight as a function of protein concentration was measured for both cardiac and skeletal S1 in a device constructed with a Lexel Model 85 0.5-W argon ion laser, a temperature-regulated cuvette holder, and a 1P21 photomultiplier tube mounted on an angular table. The high voltage for the PM dynode was supplied by a Kepco, Inc., dc regulated power supply. The 476.5-nm line of the laser operated in the light control mode was isolated with a temperature-compensated intracavity prism (Lexel Model 500), and the power was typically 50 mW. The photomultiplier current was converted to voltage and RC filtered with the Durrum Model D-131 amplifier. The amplifier output was recorded as a function of time on a two-pen Linear Instruments Model 232 chart recorder. The laser intensity monitor photodiode output was simultaneously recorded with the sample scattered intensity so that any variation of laser output could be corrected for. This correction was usually less than 3% over any 3-h period.

The light-scattering photometer was calibrated at the beginning and end of each experiment with Ludox HS-40 (Du Pont). The Ludox was prepared for use by diluting 1–140 in 0.1 M KCl and 0.01 N HCl; the diluted Ludox was then centrifuged at 30000g for 1 h, and the supernatant carefully was removed and stored in a dust-free environment. A sample of the 0.1 M KCl and 0.01 N HCl solvent was treated in a similar fashion to be used for a solvent background in the calibration. This dilution of Ludox gave a scattered intensity comparable to the highest concentration of S1 used. The Rayleigh ratio, R_c, for Ludox was determined in a 5-cm path length cell in a Cary 118 spectrophotometer by employing the relationship given by Herbert & Carlson (1971): $R_c = 3(OD)/[8\pi(\log e)l]$, where OD is the optical density of the Ludox minus the OD of the solvent at the laser wavelength, and l is the path length of the cuvette used. The Rayleigh ratio, R_s, for each of the protein solutions was then determined by using the following relationship, also given by Herbert & Carlson (1971): $R_s = R_c(A_s/A_c)$, where A_s is the scattered intensity of the sample minus the buffer scattering and A_c is the scattered intensity of the Ludox minus the Ludox solvent. The scattered intensities were determined at 90° to the incident (vertical polarization of incident laser beam) with a 1-cm^2 cuvette, and the sample and Ludox scattering intensities were recorded with the same incident laser intensity and photomultiplier dynode voltage. The dynode voltage was adjusted so that the chart recorder output of the Ludox solvent scattering was at midrange, and a set of four calibrated neutral density filters was then used to attenuate the incident beam

so that the scattered intensities at the photomultiplier tube were approximately equal for all samples. This procedure using neutral density filters thus avoided problems of nonlinear amplification by the PM tube over the wide range of observed scattered intensities and avoided complications associated with variation of the PM dynode voltage and allowed the calibration for each experiment to be performed with the same instrument settings used for sample determination.

The reciprocal of the apparent weight-average molecular weight (M_{app}) for small molecules is given by $Kc/R_s = 1/M_{app} = (1 + Bc)/M_w$, where K is an optical constant for vertically polarized incident light and is given by $4\pi^2 n_0^2 (\partial n/\partial c)^2/(N_0\lambda^4)$, c is the concentration of protein in g/mL, R_s is the Rayleigh ratio for concentration c in units of cm^{-1}, M_w is the weight-average molecular weight in units of g/mol, B is the second virial coefficient in units of mL/g, n_0 is the refractive index of the solvent, $\partial n/\partial c$ is the differential refractive index of the protein in units of mL/g, N_0 is Avogadro's number, and λ is the wavelength of the incident light in units of cm. For a monomer–dimer equilibrium, $Kc/R_s = (1 + Bc)/[M_w[2 - g(c)]]$, where $g(c)$ is the fraction of monomer given by $g(c) = [-1 + (1 + 4K_{M,D}c)^{1/2}]/(2K_{M,D}c)$, where $K_{M,D}$ is the monomer–dimer equilibrium constant in units of mL/g and it is assumed that the monomer and dimer have identical second virial coefficients.

The differential refractive index, $\partial n/\partial c$, was measured for all proteins or protein + ATP in a Model RF-600 differential refractometer (C. N. Wood Manufacturing Co.) that had been calibrated with KCl as suggested by the manufacturer by using the 546- and 436-nm lines of a mercury lamp. The calibrations for the argon ion laser lines were then obtained by linear interpolation. At 476.5 nm, the differential refractive index was 0.2079 and 0.2135 mL/g for bovine cardiac S1 and rabbit skeletal S1, respectively, in 50 mM BTP, 10 mM $MgCl_2$, and 0.1 mM DTT, pH 7.0, at 20 °C. The addition of ATP to 60 μM had no measurable effect on $\partial n/\partial c$ for cardiac S1.

All proteins were filtered directly into the scattering cuvette through 0.22-μm Millex filters (Millipore Corp.). The absorbance from an aliquot of each scattering sample was measured, and the protein concentration was determined from $A_{280}^{1\%} = 7.5\ cm^{-1}$. Another scattering sample was used to obtain $\partial n/\partial c$. The protein samples were stored on ice and allowed to thermally equilibrate to 20 ± 0.1 °C in the brass block temperature-regulated cell holder. Dust discrimination was done visually from the chart recorder trace since the dust spikes clearly stand out from the minimum scattering over the 10–15-min measurement period used to be sure that temperature equilibration had been reached and that a minimum scattering had been obtained.

Results

The variation of the fast- and slow-phase rate constants is given in Figure 1 for cardiac S1 as a function of S1 concentration for a fixed ATP concentration of 60 μM. The fast- and slow-phase rate constants are given for three concentrations of KCl, 0.0, 0.1, and 0.5 M. It can be seen that the largest rate constants are observed for the no-salt case at low S1 concentration and that the apparent ATP binding constants decrease with increasing KCl concentration. The observed rate constants reflect primarily binding as the ATP concentration is well below that needed to reach the plateau region in the observed rate constant. However, at high S1 concentrations, the rate constants for 0.1 M KCl are greater than those for either 0.0 or 0.5 M KCl. The dashed lines were calculated as described under Materials and Methods and are the expected single-exponential rate constants taking into account

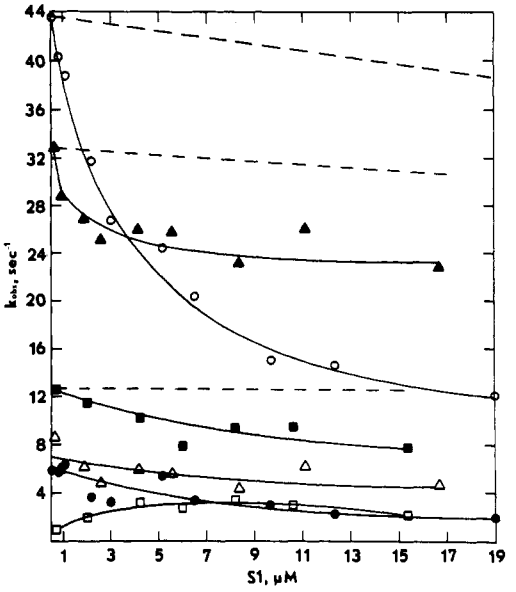

FIGURE 1: Kinetic data for constant ATP and variable cardiac S1. A plot of k_{fast} (○) and k_{slow} (●), no added KCl; k_{fast} (▲) and k_{slow} (△), 0.1 M KCl; and k_{fast} (■) and k_{slow} (□), 0.5 M KCl, for cardiac S1 as a function of S1 concentration after mixing. The concentration of ATP was held constant at 60 μM after mixing in the case of 0.0 and 0.1 M KCl and 56 μM in the case of 0.5 M KCl. The buffer was 50 mM BTP, variable KCl, 10 mM $MgCl_2$, and 0.1 mM DTT, pH 7.0, and the experiments were conducted at 20 °C. The solid lines are drawn for continuity of the data only, and the dashed lines as explained in the text are calculated for the departure from strict pseudo-first-order conditions for ATP with respect to S1.

the non-pseudo-first-order behavior due to the fact that ATP is not in great excess for all S1 concentrations. The decrease in rate constant with increasing S1 concentration is clearly not due to second-order behavior. For all KCl concentrations, the larger rate constants at lower S1 concentrations are an indication that the less aggregated form of S1 has a larger ATP binding rate constant than the more aggregated form at higher S1 concentrations. The aggregation phenomena are clearly reversible because the fast- and slow-phase rate constants would be independent of S1 concentration if there were not a reversible aggregation.

The results of the second type of experiment where the ATP/S1 ratio is held fixed at 3.6 are shown in Figure 2 as a function of ATP concentration. The fast- and slow-phase rate constants are given for three KCl concentrations, 0.0, 0.1, and 0.5 M. The simulation for non-pseudo-first-order behavior is given by the dashed lines. The simulated curves and resulting dashed lines are calculated by using the same second-order constants as in Figure 1. The simulated data could not be resolved into two exponentials, and the single-exponential fits as a function of varying ATP and S1 concentrations give a straight line dependence for k_{obsd} with a slope smaller than one would expect given the input second-order rate constant for the simulation. The 0.1 M KCl data again give larger rate constants at high ATP and S1 concentrations than either 0.0 or 0.5 M KCl. The apparent plateau of the rate constants at high concentrations of ATP and S1 gives an estimate of the ATP binding constant for the more aggregated form of S1. In these experiments, nucleotide-induced aggregate dissociation is limited because the ATP concentration is kept sufficiently low so that at high S1 concentrations the rate constant becomes independent of ATP and approximates the binding of ATP to the more aggregated form.

The fractions of fast phase for the experiments in Figures 1 and 2 are given in parts A and B of Figure 3, respectively. In Figure 3A, the fraction fast phase varies from 0.8 to 0.6

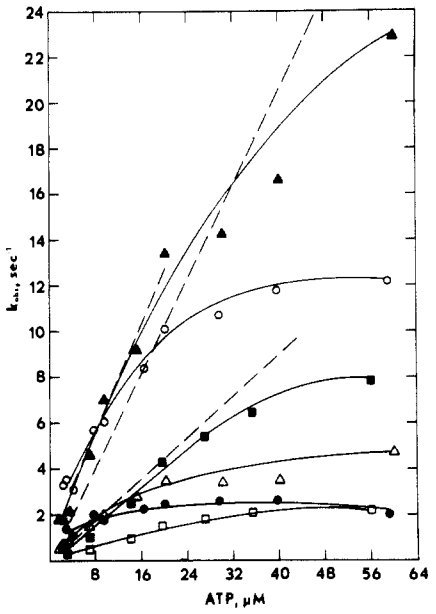

FIGURE 2: Kinetic data for a fixed ATP to cardiac S1 ratio. Plots of k_{fast} (○) and k_{slow} (●), no added KCl; k_{fast} (▲) and k_{slow} (△), 0.1 M KCl; and k_{fast} (■) and k_{slow} (□), 0.5 M KCl, for cardiac S1 as a function of the ATP concentration after mixing with the ratio ATP/S1 fixed at 3.6 for all concentrations of KCl are given. The buffer was 50 mM BTP, various KCl, 10 mM $MgCl_2$, and 0.1 mM DTT, pH 7.0, and the experiments were conducted at 20 °C. The solid lines are drawn for continuity of the data only, and the dashed lines as explained in the text are calculated for the departure from strict pseudo-first-order conditions for ATP with respect to S1.

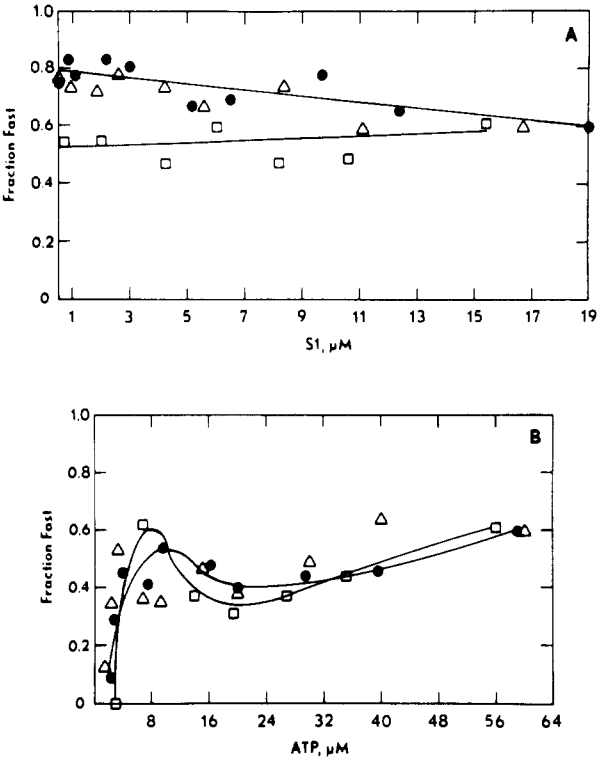

FIGURE 3: Relative contribution of the fast kinetic phase as a function of cardiac S1 concentration. (A) Fraction fast phase for 0.0 M KCl (●), 0.1 M KCl (△), and 0.5 M KCl (□) for cardiac S1 as a function of S1 concentration after mixing for ATP held constant at 60 μM after mixing in the case of 0.0 and 0.1 M KCl and 56 μM for 0.5 M KCl. The data given here and in Figure 1 are from a corresponding two-exponential fit. The solid lines are drawn for continuity of the data only. (B) Fraction fast phase for 0.0 M KCl (●), 0.1 M KCl (△), and 0.5 M KCl (□) for cardiac S1 as a function of the ATP concentration after mixing with the ratio ATP/S1 fixed for all concentrations of KCl. The data given here and in Figure 2 are from a corresponding two-exponential fit. The solid lines are drawn for continuity of the data only.

for [S1] = 0.5 to 19 μM, respectively, for both 0.0 and 0.1 M KCl. If the rate of monomer–dimer equilibration is slower than the rate of ATP binding, then we may calculate the apparent dissociation constant from $K_{D,M} = 2R^2P_T/(1 - R)$, where R is the fraction rapid and P_T is the total S1 concentration. For 0.0 and 0.1 M KCl we obtain $K_{D,M}$ = 3.4 μM for 0.5 μM S1 and $K_{D,M}$ = 34 μM for 19 μM S1. Since $K_{D,M}$ should be a constant for all concentrations of S1, we can conclude that the aggregation is not a simple monomer–dimer equilibrium or that the equilibration between these two forms is not slow compared to the rate of ATP binding. The estimated accuracy in the fractions is ~10%, and the behavior in 0.5 M KCl is clearly different from that in either 0.0 or 0.1 M KCl.

The behavior of the fraction fast phase for the ratio ATP/S1 = 3.6 is quite complex (Figure 3B). The fast-phase amplitudes are quite similar for all three KCl concentrations, and they all show a decrease and then increase in the region 8–24 μM in ATP. Since both the S1 and ATP concentrations are varied in this experiment, there are obviously at least two different competing processes taking place: the amount of aggregated S1 increases with protein concentration, and ATP induces interconversion between the aggregated forms in competition with binding to the active site. Both processes are taking place on the same time scale. The total fluorescence enhancements for cardiac S1 given here are constant at 33–34% for all variations of protein and nucleotide.

Similar experiments with variation of protein concentration and fixed ATP as well as varying both but keeping the ATP/S1 ratio fixed were carried out with rabbit skeletal S1 (A1). For ATP fixed at 60 μM, the data are monophasic and the k_{obsd} varies from 57 to 50 s^{-1} for S1 concentrations varying from 1 to 17 μM. The solid line in Figure 4A is from the simulation for non-pseudo-first-order behavior (Materials and Methods) and represents the observed trend very well. The corresponding experiment with the ATP/S1 ratio fixed at 3.6 (Figure 4B) is also fit within experimental error with the same apparent second-order binding constant used in the simulation in Figure 4A. The pseudo-first-order constants obtained for rabbit S1 (A1) agree quite well with those of Johnson & Taylor (1978) at 60 μM ATP. Their data are for a lower ionic strength, and they have shown that the apparent second-order binding constant for ATP decreases with increasing KCl. The total fluorescence enhancement corresponding to the data in Figure 4 for rabbit S1 (A1) is the same for all variations of ATP and S1 and is 33–34%. The fact that rabbit S1 displays such simple behavior as a function of S1 concentration shows that the behavior of bovine cardiac S1 is clearly more complicated and that the heterogeneity in cardiac S1 is directly related to aggregation.

The steady-state rate constant, k_4, for cardiac S1 is clearly complex, with the data presented in Figure 5 from experiments measuring the single turnover of ATP. The rate constant in 0.0 M KCl is larger for the aggregated form of cardiac S1, whereas in 0.5 M KCl, the opposite is true. However, because ATP causes interconversion of the aggregated forms of S1, and because the single-turnover experiments cannot be resolved into two exponentials for the fluorescence decay following the initial ATP binding, it is not possible to clearly establish which form of S1 is more active except to say that the aggregation of cardiac S1 does effect k_4. The total fluorescence enhancement of ATP-bound myosin relative to myosin in these experiments is 33–34%.

A simple minimum mechanism can be constructed which

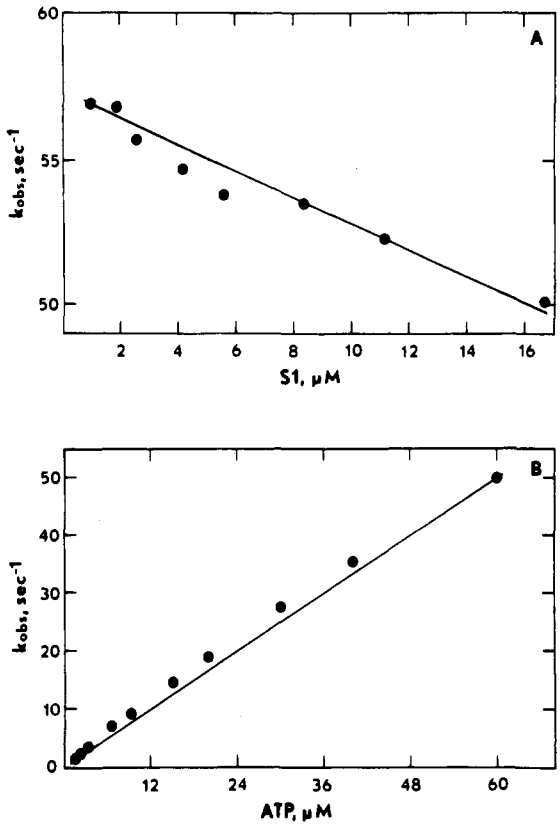

FIGURE 4: (A) A plot of k_{obsd} for rabbit skeletal S1 as a function of the S1 concentration after mixing. The ATP concentration was held constant at 60 μM after mixing. The buffer was 50 mM BTP, 0.1 M KCl, 10 mM $MgCl_2$, and 0.1 mM DTT, pH 7.0, and the experiments were conducted at 20 °C. The solid line as explained in the text is calculated for the departure from strict pseudo-first-order conditions for ATP with respect to S1. (B) A plot of k_{obsd} for rabbit skeletal S1 as a function of ATP concentration after mixing with the ratio ATP/S1 fixed at 3.6. The buffer is the same as that in (A). The solid line as explained in the text is calculated for the departure from strict pseudo-first-order conditions for ATP with respect to S1.

will describe the heterogeneity in the kinetics of ATP binding to cardiac S1:

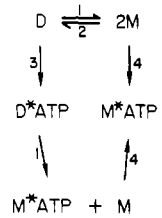

where D is dimeric S1, M is monomeric S1, M*ATP is the tryptophan fluorescence enhanced form of monomeric S1, and D*ATP is the dimer form with one ATP bound with fluorescence enhancement, i.e., M–M*ATP, and the fluorescence of M*ATP in the dimer is assumed to be the same as that in the monomeric form of S1. For the simplest case, the rate constants for dissociation of both forms of the dimer (D and D*ATP) were assumed to be equal (k_1), and the rate constant for ATP binding to the dimer (k_3) was different than that for ATP binding to the monomer (k_4). Runge-Kutta numerical integration of the simultaneous differential equations for the above mechanism was carried out by using the algorithm of Gear (1971). The four rate constants (given by 1–4 above) were varied to give an approximate fit to the data from the 0.0 M KCl experiments for cardiac S1. The derived (solid or dashed lines) and measured fast- and slow-phase rate constants are given in Figure 6 for the experiments done with

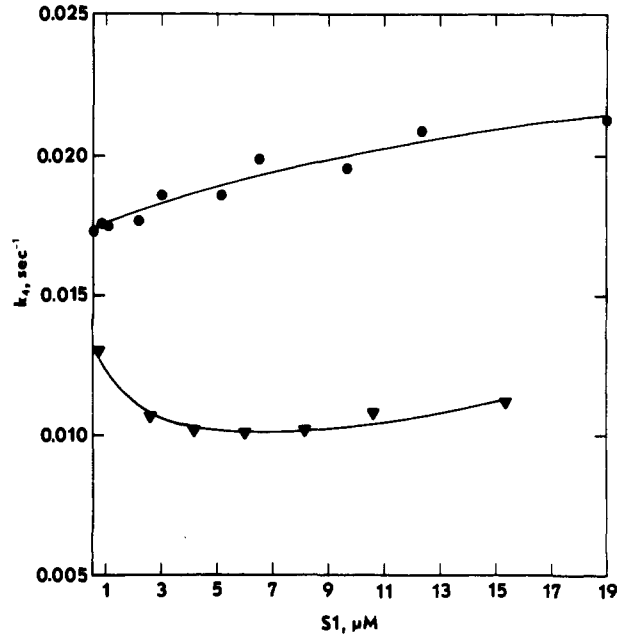

FIGURE 5: A plot of k_4, the steady-state rate constant, for 0.0 M KCl (●) and 0.5 M KCl (▼) as a function of the cardiac S1 concentration after mixing. These constants are derived from single-turnover experiments in the stopped-flow apparatus by mixing S1 with stoichiometric concentrations of ATP. The buffer was 50 mM BTP, 0.0 M KCl or 0.5 M KCl, 10 mM $MgCl_2$, and 0.1 mM DTT, pH 7.0, and the experiments were done at 20 °C. The solid lines are given for continuity of data only.

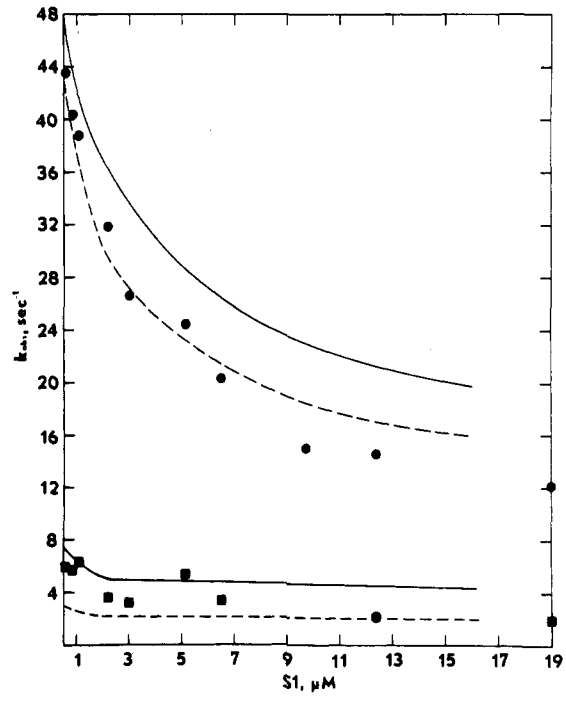

FIGURE 6: A plot of k_{fast} (●) and k_{slow} (■) for cardiac S1 as a function of S1 concentration after mixing. The concentration of ATP was held constant at 60 μM after mixing. The buffer was 50 mM BTP, 0.0 M KCl, 10 mM $MgCl_2$, and 0.1 mM DTT, pH 7.0, and the experiments were conducted at 20 °C. The solid lines are calculated for the model given in the text for a dimer–monomer dissociation constant $K_{D,M}$ = 4 μM, and the dashed lines are for $K_{D,M}$ = 2 μM.

[ATP] fixed and varying [S1] and in Figure 7 for the experiments done with the ratio ATP/S1 fixed at 3.6 (KCl was 0.0 M in both figures). The solid curves are for the rate constant set $k_1 = 4\ s^{-1}$, $k_2 = 1 \times 10^6\ M^{-1}\ s^{-1}$, $k_3 = 1.7 \times 10^5\ M^{-1}\ s^{-1}$, and $k_4 = 1 \times 10^6\ M^{-1}\ s^{-1}$ (i.e., $K_{D,M} = k_1/k_2 = 4\ \mu M$). The dashed lines are for the set $k_1 = 2\ s^{-1}$, $k_2 = 1 \times 10^6\ M^{-1}$

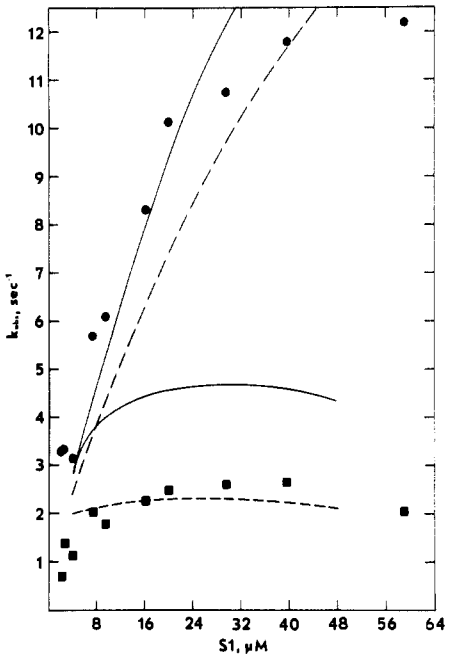

FIGURE 7: A plot of k_{fast} (●) and k_{slow} (■) for cardiac S1 as a function of ATP concentration after mixing with the ratio ATP/S1 fixed at 3.6. The buffer was 50 mM BTP, 0.0 M KCl, 10 mM $MgCl_2$, and 0.1 mM DTT, pH 7.0, and the experiments were conducted at 20 °C. The solid lines are calculated for the model given in the text for a dimer–monomer dissociation constant $K_{D,M}$ = 4 μM, and the dashed lines are for $K_{D,M}$ = 2 μM.

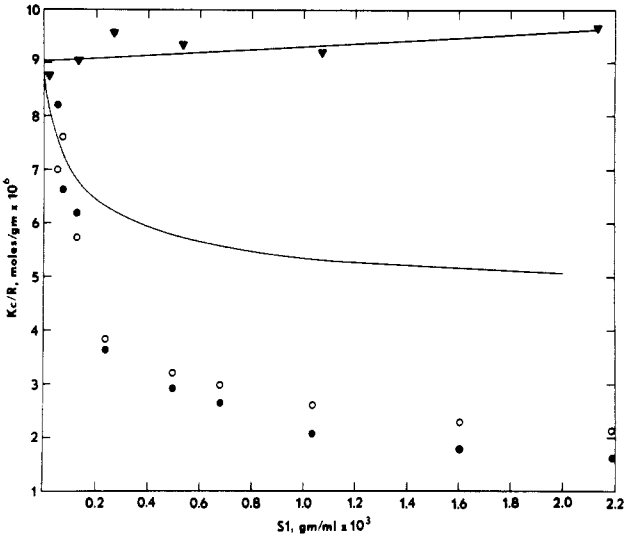

FIGURE 8: A plot of Kc/R, the reciprocal of the apparent weight-average molecular weight, as a function of the S1 concentration for cardiac S1 (●), cardiac S1 + 60 μM ATP (○), and rabbit skeletal S1 (▼). The buffer was 50 mM BTP, 0.0 M KCl, 10 mM $MgCl_2$, and 0.1 mM DTT, pH 7.0. The measurements were made at 20 °C, and the incident wavelength was 476.5 nm. The solid curve is calculated for a dimer–monomer dissociation constant $K_{D,M}$ = 2 μM and the second virial coefficient B = 0. The solid straight line through the rabbit skeletal S1 data is a linear least-squares fit as given in the text.

s^{-1}, $k_3 = 1.7 \times 10^5$ M^{-1} s^{-1}, and $k_4 = 1 \times 10^6$ M^{-1} s^{-1} (i.e., $K_{D,M}$ = 2 μM). The quality of the fit to the data in Figures 6 and 7 is reasonable for k_1 = 2 s^{-1} ($K_{D,M}$ = 2 μM). The fraction fast phase remains large (Figure 3) even at high protein concentrations because ATP promotes the formation of monomeric S1 in the model given. In principle, the slow phase could be made the only species present at high S1 concentrations (>20 μM) and low ATP (<30 μM); however, under these conditions the kinetics of ATP binding would no longer be pseudo first order.

The simple mechanism proposed above is obviously not the only mechanism that could describe the biphasic kinetics for cardiac S1. The assumption of a fluorescence change with ATP binding to the dimer form is necessary because its absence leads to a lag phase in the simulated fluorescence change at high S1 concentrations. For simplicity, the fluorescence change for the binding of one ATP to the dimer is made to be the same as for the binding of one ATP to monomeric S1. This type of model suggests that dissociation of the aggregated form of S1 is induced by ATP binding to the active site of one S1 in the aggregate. However, as far as the simulation is concerned, the site of ATP binding in the dimer is not specified, and it is only necessary that a fluorescence change takes place when ATP binds.

It is well established that the binding and rapid hydrolysis of ATP in rabbit skeletal S1 occur in at least two steps with fluorescence enhancement, and a model for the aggregation-dependent process for cardiac S1 should include more steps than the simple model given above. The light-scattering results presented below indicate an even more complicated model should be used since there are more than two aggregated forms of cardiac S1. The model presented above is therefore over-simplified, but it does represent the data well with only four rate constants and can be used as a basis for understanding the aggregation phenomena.

The results of the static light-scattering experiments fully support the interpretation of aggregation-linked kinetic heterogeneity in cardiac S1. The results presented in Figure 8 clearly show that cardiac S1 is aggregated and that rabbit S1 (A1) is not. The experiments also show that 60 μM ATP induces dissociation of the cardiac aggregates. However, the experiments do not show that ATP induces dissociation on the same time scale as ATP binding. A minimum of 30 s was needed between injection of a concentrated ATP solution and the first measurement of scattering, and a further 2 min was needed to ensure that the scattering was stable. The data are corrected for the very small volume change for the ATP addition. For none of the observations (2 min) could a slow drift be seen that would be comparable to the steady-state turnover of ATP, and thus the decrease of the weight-average molecular weight must be primarily due to ATP. Further observation for 15 min showed no change in the scattered intensity.

Extrapolation to zero concentration yields a value of (1.15 ± 0.02) × 10^5 for the molecular weight of chymotryptic cardiac S1. The experiments also show that cardiac S1 undergoes reversible aggregation to higher molecular weight species than dimers. The solid curve in Figure 8 is calculated for a $K_{D,M}$ of 2 μM with the second virial coefficient equal to zero. Cardiac S1 may exist in the form of tetramers at 2 mg/mL S1 concentration, depending on the value of the second virial coefficient. With the present data, it is not possible to determine the multiple equilibrium constants that must exist for the aggregation of cardiac S1. It should be noted that $NaDodSO_4$–polyacrylamide electrophoresis shows the absence of actin contamination and that the heaviest component present in our preparation of cardiac S1 is the ~90 000 molecular weight heavy chain of S1.

The rabbit skeletal S1 (A1) light-scattering data were fit by linear least-squares analysis to $Kc/R = (1 + Bc)/M_w$, and the molecular weight was determined as (1.11 ± 0.02) × 10^5 and the second virial coefficient as 199 mL/g. The value for the molecular weight of rabbit S1 (A1) agrees quite well with that of Margossian & Stafford (1979) determined in the ultracentrifuge [(1.15 ± 0.02) × 10^5]. They suggested that gel permeation chromatography was necessary to remove low

molecular weight fragments which was not done in our case and may account for the slightly lower molecular weight obtained.

Discussion

It is clear from the work reported here that bovine cardiac S1 undergoes reversible aggregation in solution and that this aggregation is the reason for the observed biphasic kinetics (Taylor & Weeds, 1976). The light-scattering results support the simple mechanism proposed to account for the S1 concentration dependence of the ATP binding process as well as the fact that the kinetics are biphasic. The light-scattering results with ATP also confirm the ATP-dependent interconversion of aggregated cardiac S1. However, the light-scattering results also show that any mechanism proposed must include higher aggregates. As pointed out under Results, the simple model proposed is oversimplified because the ATP binding and rapid hydrolysis must occur in at least two steps and the light-scattering results indicate that more than monomer and dimer species of cardiac S1 must be included. The contrast between the simple behavior of rabbit skeletal S1 (A1) in both the kinetic and light-scattering studies and the solution behavior of bovine cardiac S1 is quite striking. The steady-state rate constant, k_4, has been shown in this work to depend on protein concentration, and any future work on cardiac S1 which uses this constant as a measurable parameter should take into account the aggregation of cardiac S1. Until the complicated solution properties of cardiac S1 are completely resolved, further mechanistic studies will have to be interpreted with caution.

Acknowledgments

We thank Bill Kleese for excellent technical assistance and Howard White for many helpful discussions.

References

Foss, S. D. (1970) *Biometrics 26*, 815.
Gear, C. W. (1971) in *Numerical Initial Value Problems in Ordinary Differential Equations*, Chapter 2, Prentice-Hall, Englewood Cliffs, NJ.
Greenstadt, J. (1967) *Math. Comput. 21*, 360.
Herbert, T. J., & Carlson, F. D. (1971) *Biopolymers 10*, 2231.
Johnson, K. A., & Taylor, E. W. (1978) *Biochemistry 17*, 3432.
Margossian, S. S., & Stafford, W. F. (1979) *Biophys. J. 25*, 20a.
Taylor, R. S., & Weeds, A. G. (1976) *Biochem. J. 159*, 301.
Weeds, A. G., & Taylor, R. S. (1975) *Nature (London) 257*, 54.
Weeds, A. G., & Pope, B. (1977) *J. Mol. Biol. 111*, 129.
Weeds, A. G., Hall, R., & Spurway, N. C. (1975) *FEBS Lett. 49*, 320.

Phosphorus-31 Nuclear Magnetic Resonance Studies of Adenosine 5′-Triphosphate Bound to a Nitrated Derivative of G-Actin†

Manfred Brauer and Brian D. Sykes*

ABSTRACT: G-Actin was nitrated with tetranitromethane to form a relatively nonpolymerizable derivative. The ^{31}P NMR spectrum of ATP bound to the nitrated G-actin derivative does not differ significantly from that of ATP bound to unmodified G-actin, indicating that the nitration of Tyr-69 does not appreciably affect the ATP binding site. The relaxations times, T_1 and T_2, for the ^{31}P resonances of protein-bound ATP were measured as a function of magnetic field strength to separate the contributions of dipole–dipole and chemical shift anisotropy relaxation mechanisms. At high magnetic field strengths (8.4 T), chemical shift anisotropy was found to account for about 90% of the spin–spin relaxation rate ($1/T_2$) and about 80% of the spin–lattice relaxation rate ($1/T_1$) for all three phosphates. The effects of cross-relaxation between ^{31}P and ^{1}H nuclei are shown to be negligible for protein-bound phosphates in the nonextreme narrowing limit. On the basis of the contribution of chemical shift anisotropy to T_1 and T_2, rotational correlation times of 41, 40, and 44 ns were determined for the γ-, α-, and β-phosphates of bound ATP. Since the theoretical tumbling time for G-actin is about 36 ns, these correlation times indicate that each phosphate of ATP in the G-actin–ATP complex is tightly bound with no appreciable rapid internal mobility. Chemical shift anisotropy factors $(\Delta\sigma)(1 + \eta^2/3)^{1/2}$ were 240, 260, and 260 ppm for the bound γ-, α-, and β-phosphates, respectively. These anisotropies are higher than would be expected from model compounds and reflect interactions between the G-actin and its bound ATP. At lower magnetic field strengths, the line widths of the protein-bound phosphates are appreciably narrower and the ^{31}P–^{31}P spin coupling constants can be observed. ^{31}P NMR (36.4 MHz) spectra show a decrease in $^{2}J_{P_\alpha,P_\beta}$ from 19.6 Hz for free ATP to 12 ± 2 Hz for actin-bound ATP, also indicating some interaction between the ATP and protein.

Actin plays a central role in the structure and function of muscle. It is the major structural component of the thin filament of muscle (Oosawa & Kasai, 1971; Engel et al., 1977). Actin interacts with tropomyosin and troponin in the calcium-mediated control system for muscle contraction (McCubbin & Kay, 1980; Mannherz & Goody, 1970; Ebashi & Ebashi, 1965). The interaction of actin with the myosin heads of the thick filaments produces the force which drives the interdigitating thin and thick filaments past each other during muscle contraction (Huxley, 1969; Mannherz & Goody, 1970). Actin has also been found in virtually all nonmuscle eukaryotic cells (Clarke & Spudich, 1977), and

† From the Medical Research Council Group on Protein Structure and Function and the Department of Biochemistry, University of Alberta, Edmonton, Alberta, Canada T6G 2H7. *Received April 9, 1981.* This research was supported by the Muscular Dystrophy Association of Canada (Postdoctoral Fellowship to M.B.) and the Medical Research Council of Canada (Group on Protein Structure and Function). A preliminary report of this work was presented at a meeting of the American Society of Biological Chemists, St. Louis, MO, June 1981.

0006-2960/81/0420-6767$01.25/0